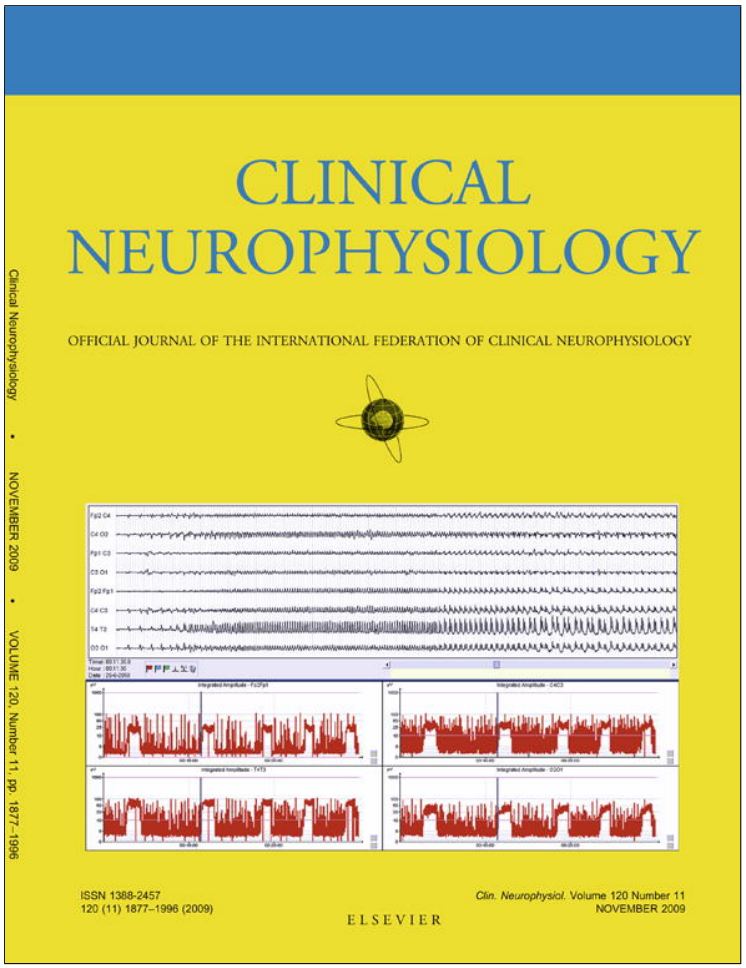

Clinical Neurophysiology 120 (2009) 1958–1970

Contents lists available at ScienceDirect

Clinical Neurophysiology

journal homepage: www.elsevier.com/locate/clinph

MEG's ability to localise accurately weak transient neural sources

Christos Papadelis [a,b,*], Vahe Poghosyan [c,a], Peter B.C. Fenwick [a], Andreas A. Ioannides [a,c]

[a] Laboratory for Human Brain Dynamics, Brain Science Institute (BSI), RIKEN, 2-1 Hirosawa, Wako-shi, Saitama 351-0198, Japan
[b] Laboratory of Functional Neuroimaging, Center for Mind/Brain Sciences (CIMeC), University of Trento, Via delle Regole 101, 38060 Mattarello (TN), Italy
[c] Laboratory for Human Brain Dynamics, AAI Scientific Cultural Services Ltd., Office 501, Galaxias Building Block A, 33 Arch. Makarios III Avenue, 1065, Nicosia, Cyprus

ARTICLE INFO

Article history:
Accepted 31 August 2009
Available online 25 September 2009

Keywords:
MEG
High Frequency Oscillations
Localisation
Phantom
ECD
MUSIC
SAM
MFT

ABSTRACT

Objective: To investigate the accurate localisation of weak, transient, neural sources under conditions of varying difficulty.
Methods: Multiple dipolar sources placed within a head-shaped phantom at superficial and deep locations were driven separately or simultaneously by a short-lasting current with varied amplitudes. Artificial MEG signals that were very similar to the human High Frequency Oscillations (HFO) were produced. MEG signals of HFO were also recorded from median nerve stimulation. Different inverse techniques were used to localise the phantom dipoles and the human HFO generators.
Results: The human HFO were measured around 200 and 600 Hz by using only 120 trials. The 200 Hz HFO were localised to BA3b. The superficial phantom's source was localised with an accuracy of 2–3 mm by all inverse techniques (120 trials). The 'subcortical' source was localised with an error of ~5 mm. Localisation of deeper 'thalamic' sources required more trials.
Conclusion: MEG can detect and localise weak transient activations and the human HFO with an accuracy of a few mm at cortical and subcortical regions even when a small number of trials are used.
Significance: Localizing HFO to specific anatomical structures has high clinical utility, for example in epilepsy, where discrete HFO appears to be generated just before focal epileptic activity.

1. Introduction

Fast oscillatory brain activity above 100 Hz has been attracting increasing attention concerning its potential role in normal and pathological brain function. Both animal (Jones and Barth, 1999, 2002; Jones et al., 2000) and human studies (Cracco and Cracco, 1976; Curio et al., 1994; Eisen et al., 1984; Hashimoto et al., 1996; Yamada et al., 1988) have found weak somatosensory-evoked fast oscillations, frequently called HFO. Fast oscillations are also seen preceding seizure onset in human epileptic patients (Bragin et al., 1999, 2002; Jirsch et al., 2006; Staba et al., 2002).

The HFO have been measured and localised non-invasively in humans using either electroencephalography (EEG) or MEG. Both techniques offer sub-millisecond temporal resolution required for capturing the HFO dynamics. MEG has the advantage of better localisation accuracy (Leahy et al., 1998). Curio and his colleagues (1994) were the first to record the HFO magnetically from the averaged somatosensory-evoked field (SEF), elicited by median nerve stimulation. During the M20, two apparently distinct HFO components were observed with a dominant frequency around 600 Hz (Haueisen et al., 2001), and a slower signal about 200 Hz preceding the two 600 Hz components (Haueisen et al., 2001). Two frequency bands have been described for HFO, the 'low' (low-band) from 150 to 250 Hz, and the 'high' (high-band) from 450 to 750 Hz.

Following median nerve wrist stimulation, the spatial distribution of the 600 Hz averaged SEF, was similar to that of the M20 (Curio et al., 1994). It was thus suggested that the HFO and the M20 component were generated by the same thalamocortical projection area of the primary somatosensory cortex (Curio et al., 1994; Hashimoto et al., 1996). Recent studies have found that the HFO were not restricted to the cortex, but involved subcortical

Abbreviations: Av-ECD, Equivalent Current Dipole on averages; ECD, Equivalent Current Dipole; ECG, electrocardiogram; EEG, electroencephalography; EOG, electro-oculogram; GOF, goodness of fit; HFO, high frequency oscillation; ICA, independent component analysis; ITS, intertrial synchronization index; LE, localisation error; LGN, lateral geniculate nucleus; MEG, magnetoencephalography; MFT, Magnetic Field Tomography; MLS, multiple local spheres; MTH, motor threshold; MUSIC, MUltiple SIgnal Classification; NP, noise power; S1, primary somatosensory area; SAM, Synthetic Aperture Magnetometry; SEF, somatosensory-evoked field; SMA, supplementary motor area; SNR, signal-noise-ratio; SP, signal power; SPM, statistical parametric map; SS, single sphere; ST, single trial; STH, sensory threshold.

* Corresponding author. Address: Laboratory of Functional Neuroimaging, Center for Mind/Brain Sciences (CIMeC), University of Trento, Via delle Regole 101, 38060 Mattarello (TN), Italy. Tel.: +39 0461 88 2779; fax: +39 0461 88 3066.
E-mail addresses: christos.papadelis@unitn.it, cpapad@med.auth.gr (C. Papadelis).

1388-2457/$36.00 © 2009 International Federation of Clinical Neurophysiology. Published by Elsevier Ireland Ltd. All rights reserved.
doi:10.1016/j.clinph.2009.08.018

and even subthalamic sites (Gobbelé et al., 1998, 1999, 2004). With single moving dipole analysis, the HFO generators were localised as an almost continuous set of sources, activated almost simultaneously. This set of dipoles extended from the brainstem, through the thalamus to the contralateral somatosensory cortex (Gobbelé et al, 2004).

MEG studies have provided some insights into the location of HFO generators. However the localisation accuracy of MEG is debated on theoretical and practical grounds, particularly when deep and multiple sources are involved. At the theoretical level, the biomagnetic inverse problem, i.e. the task of determining the generators from the measurements has no unique solution, since any given magnetic field distribution can be generated by an infinite number of source configurations (von Helmholtz, 1853). Additional information is needed to impose constraints, and thus lead to a unique solution. Many source localisation methods are available each using different constraints.

The HFO generators have so far been studied using mainly ECD source analysis applied to the average MEG signal from very large number, often thousands of trials (Curio et al., 1994, 1997; Gobbelé et al, 2004; Hashimoto et al., 1996, 1999; Norra et al., 2004; Ozaki et al., 1998) with simple head models (Gobbelé et al, 1998, 2004; Hashimoto et al., 1999). So the question remains whether MEG is able to detect and localise accurately the very weak, possibly multiple and almost simultaneously active neural sources that are responsible for the generation of HFOs. If so, which source localisation methods are more appropriate and how many trials are necessary for reliable source estimation.

An effective and simple way to validate the localisation accuracy of MEG for cortical, subcortical and deep current sources has been to use head-shaped phantoms. Phantoms allow the generation of magnetic signals with similar features to the ones measured during MEG experiments with healthy subjects or in pathological conditions like epilepsy. In phantom studies, the location and temporal dynamics of the underlying sources are known. Saline-filled spherical phantoms (Hansen et al., 1988; Papadelis and Ioannides, 2007; Sutherling et al., 2001; Vrba and Robinson, 2000), real or constructed human skull phantoms filled with conducting gelatin (Leahy et al., 1998; Yamamoto et al., 1988), and cadaver heads (Barth et al., 1986) have been used to test MEG localisation accuracy.

The localisation accuracy of MEG for weak, transient, single and multiple sources is examined in this paper using a realistically shaped phantom with multiple, electrically isolated, dipolar sources placed at superficial and deep locations. None of the phantom studies available from the literature have so far made use of such weak transient currents. The aim was to study the detection and localisation of sources that are responsible for the generation of HFO under conditions of varying difficulty assuming superficial as well as subcortical and thalamic, single and simultaneously active generators. An artificial MEG signal was generated for this reason by activating simple dipolar sources in different but precisely determined locations inside the phantom. The sources were driven, either separately or simultaneously by weak, transient, constant current pulses of identical wave shape and frequency but with different amplitudes. It was followed the well-defined signal processing used in the literature for detecting and localising the somatosensory-evoked HFO. The SEFs of human median nerve stimulation were examined for HFO in different frequency bands. These data were used to set the phantom's dipole moments, so that the resulting MEG signal in the phantom setup had the same amplitude with the HFO at the sensor level, after filtering and averaging. The measurements with the phantom setup were then made in the usual way so that the resulting MEG signal recorded included both the contribution from the source in the phantom and the system noise which, given the stable noise levels of our system, had similar properties as the system noise in our somatosensory-evoked experiment. Four different source localisation methods (Equivalent Current Dipole (ECD), MUltiple SIgnal Classification (MUSIC), Synthetic Aperture Magnetometry (SAM), and Magnetic Field Tomography (MFT)) were used to localise the phantom dipolar sources, as well as the generators of low-band HFO.

2. Materials and methods

2.1. Somatosensory experiment

2.1.1. Subjects and measurements

Two healthy male right-handed subjects (ages: 29 and 33 yrs) participated in a somatosensory experiment. Ethical committee approval was obtained from the RIKEN Ethics Committee and subjects gave written informed consent before the experiment. The median nerve was electrically stimulated transcutaneously on the right and left wrists. Two electrodes (cathode proximal) were connected directly to the photoelectric stimulus isolation unit of our electrical stimulator (Grass Model S8800). Before the experiment, the motor threshold (MTH, the minimal stimulus intensity required to produce thumb movement), and the sensory threshold (STH, the minimal stimulus intensity corresponding to the level at which the subject was just able to feel a train of stimulus pulses, repeated four times) were determined for each wrist. During the experiment, the subject was comfortably seated inside the magnetically shielded room without moving his head, which was inside the helmet-like bottom part of the dewar. The stimulated arm was well covered to prevent cooling throughout the recording session.

Constant current stimuli with a duration of 0.2 ms, and normally distributed pseudo-randomized interstimulus interval with mean of 600 ± 100 ms were used. The stimulus intensity M was $M = MTH + 0.25 \cdot \Delta$, where $\Delta = MTH - STH$ (Ioannides et al., 2002). MTH and STH stimuli were 5.4 ± 1.2 mA (mean ± SD) and 2.8 ± 0.8 mA respectively. A grounded band was placed round the forearm above the stimulating electrodes in order to minimize the artifactual magnetic fields caused by the stimulus current. The subject kept his eyes open and fixated a small cross. We collected four runs, each with 120 stimuli, for the right and left wrists. Two more data runs were collected with a higher sampling rate as described below.

SEFs were recorded using the CTF (VSM MedTech Ltd.) whole head system (151 channels) at a sampling rate of 2083 Hz, together with auxiliary channels recording the vertical and horizontal electro-oculogram (EOG), and electrocardiogram (ECG). The CTF system uses radial gradiometers as primary sensors. For one subject a second experiment was carried out using the same stimulation parameters but with a high-sampling rate of 4165 Hz. As our MEG system was limited at this high frequency, it could only sample 10 sensors. The auxiliary channels were also sampled at this high frequency. The channels selected for the 4165 Hz were at, and around, the M20 extrema. Hardware filters limited the bandpass of the MEG signal below 600 Hz for the sampling rate of 2083 Hz, and below 1300 Hz for the rate of 4165 Hz. Standard CTF software was used offline to process the data digitally by using a 3rd order gradient filter, a 50 Hz notch filter (and its harmonics), and by removing the DC.

2.1.2. SEF data preprocessing

The recorded MEG signal was visually inspected for possible artifacts. The INFOMAX algorithm (Lee et al., 1999) for Independent Component Analysis (ICA) in conjunction with the EOG and ECG data was used to remove eye blink and cardiac artifacts. To separate the HFO from the underlying M20, the recorded responses

were digitally filtered in three different frequency bands: (a) 150–250 Hz, (b) 250–450 Hz (medium-band), and (c) 450–750 Hz. The selection of these frequency bands was guided by findings from previous studies (Haueisen et al., 2001). The filtered 120 trials were then averaged offline for each separate run.

2.2. Phantom experiment

2.2.1. Phantom design

A spheroid phantom designed by one of us (AAI) and fabricated by CTF (CTF Systems Inc, BC Canada) was used (Fig. 1A). The phantom was designed to have realistic features with exaggerated departures from spherical symmetry and uniformity. Each dipole placed inside the phantom was made of two gold spheres (2 mm in diameter) separated by 4 mm center to center with the dipole moment perpendicular to the long axis of the phantom (Fig. 1A – inset). The dipoles were connected to wires leading to the stimulator. The wires were insulated and twisted to produce self-canceling magnetic fields. All implanted dipoles were placed in a direction to produce mainly tangential current. A hollow plastic tube, containing the wires and supporting the dipoles, was placed into the phantom through one of the 13 holes drilled for this purpose in the plexi-glass base. Through each hole, the dipole could be inserted to any desired height. Dipoles were placed in four locations: PhS1, PhS2, PhS3, and PhS4 (Fig. 1B). They have been chosen to represent the range of generator locations, which were proposed for HFO by Gobbelé and his colleagues (2004) and could be accessed by our phantom.

The location of PhS1 corresponded to the supplementary motor area (SMA). It represented in terms of localisation difficulty the superficial primary sensory areas, such as primary somatosensory area 1 (S1), frontal eye fields, and much of the superficial, parietal and frontal areas away from the eyes. The PhS2 dipole represented a moderately deep source just behind the eyes, and the PhS3 corresponded roughly to posterior hippocampus, and represented structures like the hippocampus and amygdala. Finally, PhS4 represented thalamic, hypothalamic, and upper brainstem neural sources.

2.2.2. Current pulse stimulations

The electrical pulses for the dipoles were derived from four individually connected photoelectric stimulus isolation units (Grass Model SIU7). Isolated current sources were used to avoid current flows between simultaneously activated dipoles. The constant current that produced the magnetic fields was independent of the dipole impedance. A small resistor added in series to the twisted-pair cable provided measurements of the current applied to the dipoles. Rectangular current pulses (2 ms duration) of different amplitudes drove the dipoles. Dipole currents varied in different runs from 1 to 20 μA, in 1 μA steps, covering typical values recorded in human MEG experiments. Assuming that all the effective current was conducted along a line between the two spheres, the dipole moment ranged from 4 to 80 nA-m. The delivered pulses were triangular, due to the cables' capacitance, with a peak 2 ms after onset, and a duration of 2 ms. The moments of multiple dipoles were adjusted so that each dipole would produce a MEG signal of similar amplitude.

Our main goal was to generate an artificial MEG signal at the sensor level that after filtering at a specific frequency band and averaging looks similar with the recorded human HFOs. No assumption was made about the nature of human HFO generators. By driving the phantom's dipolar sources with current pulses, we simulated an artificial neural generator with a signal contained frequencies from a wide-band including the frequencies of human HFO (theoretically a Dirac delta function $\delta(t)$ contains all frequencies). This signal was recorded by the MEG gradiometers with added system noise. The MEG signal was not significantly affected and distorted by the system noise (Fig. 2). The recorded MEG signal was then filtered to the specific frequencies bands of interest namely 150–250 Hz and 450–750 Hz and averaged (Fig. 2 – second row for the 150–250 Hz). The close similarity between the power spectra of the artificially generated signal and the HFO ensures a close similarity between their waveforms due to a mathematical relationship (transform) between the time and frequency domain representations of signals.

2.2.3. MEG measurements with the phantom

Eighty-four runs were collected in total, 20 runs for each single dipole position (one run for each dipole current: 1–20 μA in steps of 1 μA), three runs with two simultaneously active dipoles, and one run with three. In each run, 60 s of data were collected containing 360 current pulses, with an interstimulus interval of 160 ms. Thus, for each one of the 84 configurations we collected 360 trials.

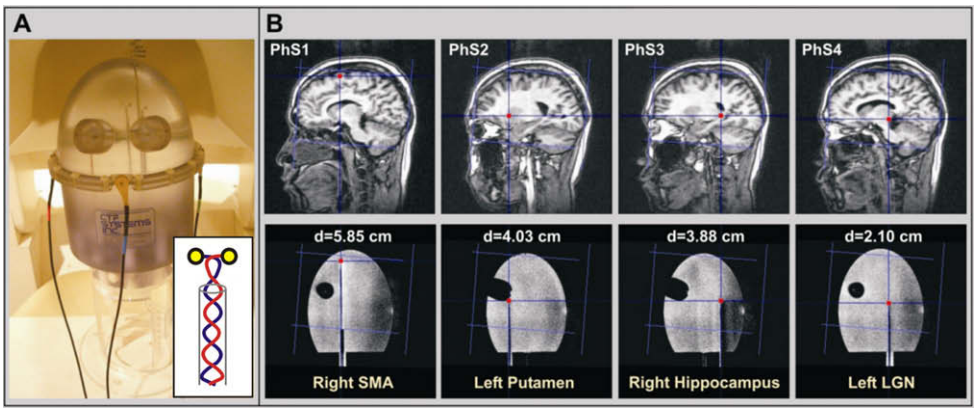

Fig. 1. (A) The spheroidal phantom placed in the helmet-like lower part of the dewar. The semicircular shadow above the phantom is the dewar with the cut away front. The total phantom height was 372.8 mm, and the plastic wall thickness 5 mm. It has a plastic spheroid globe of an elliptical vertical cross section with inner dimensions of 130 × 185.72 mm. The phantom was attached to a plexi-glass base that had a fill/drain plug. All materials in the phantom were non-ferrous for MEG sensor compatibility. The smooth inner surface was interrupted by two plastic constructions that mimicked the effect of eye sockets in a real head. Four coil locations protruded evenly spaced around the horizontal equatorial great circle of the phantom. The four coil mounting bases are on a 7.30 cm radius, and the distance to the coil centers adds a further 0.25 cm on the radius to a total of 7.52 cm. The inset shows a schematic representation of the inserted physical dipoles. (B) The four dipole locations over-plotted on the phantom's MRI scans. Each location corresponds roughly to one structure of the brain (the SMA, the putamen, the hippocampus, and the lateral geniculate nucleus (LGN)) representing the full range of difficulty in localizing generators in the brain. The distance of the dipole from the center of the spheroid, d, is printed in cm for each case.

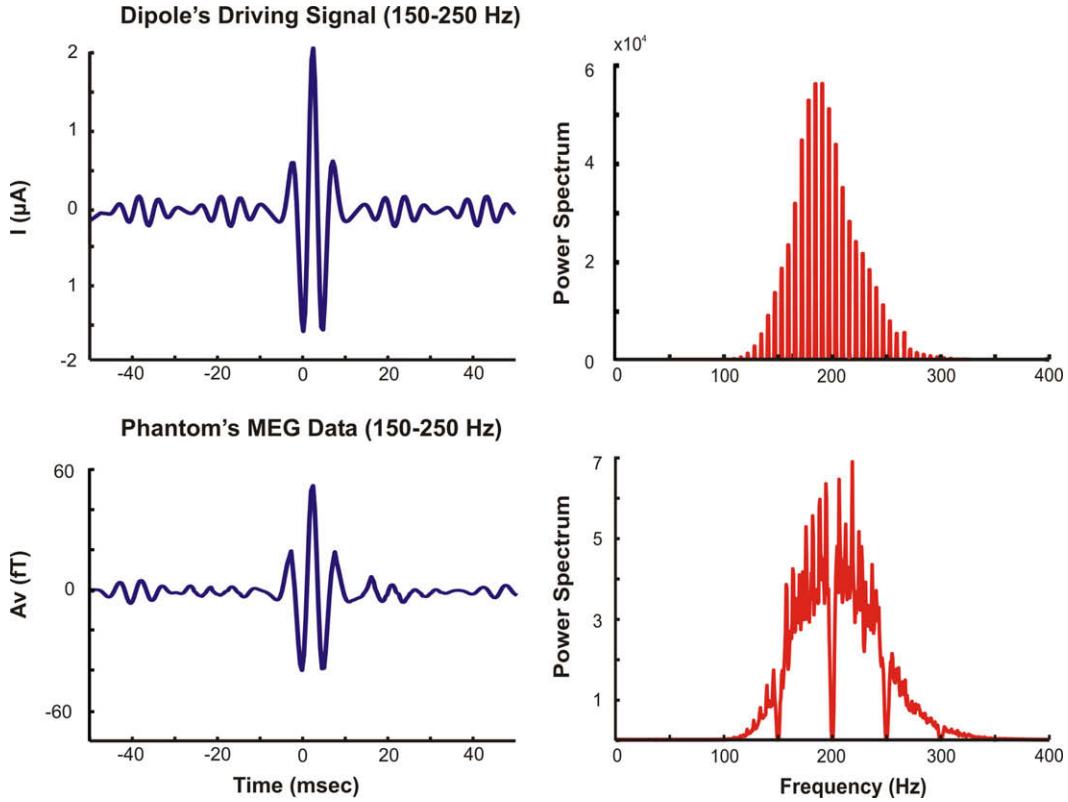

Fig. 2. (First row) The electrical current *I* (μA) driving the dipole PhS1 for the dataset of 5 μA (left) filtered in the frequency band of 150–250 Hz, and the corresponding mean power spectrum (hamming window, 4096 samples). (Second row) The averaged magnetic activity measured by virtual channel for the same dataset (after band-pass filtering of 150–250 Hz) and its corresponding power spectrum.

The spheroid phantom was placed in the dewar so that it was central and approximately 2 cm below the top. The dipoles were activated during the measurements. The phantom data were sampled at 2083 Hz (151 channels). The current stimulus and the driver signal were also recorded. In addition, measurements of high-sampling rate (4165 Hz) were recorded with 10 channels for only the superficial source. The channels selected were those that were at and surrounding the peak extrema sampled at the rate of 2083 Hz. The same preprocessing procedure was followed as for the somatosensory experiment. The trials were free from artifacts. The complete 360-trial datasets with two additional sets of the first six trials and the first 120 trials were separately averaged for each run relative to the onset of the electrical pulse.

2.2.4. MEG signal and virtual channels for SEF and phantom data

To examine the localisation of weak transient sources able to generate an artificial signal similar to the human HFO after processing, the superficial dipole (PhS1) moment in the phantom was adjusted so that the resulting MEG signals covered the range of values that were recorded during the somatosensory-evoked HFO. Since the sources of interest (either neural in SEF or artificial in phantom setup) are of focal nature producing nearly dipolar patterns, simple virtual channels were defined by estimating the difference between the mean values of the MEG signal around the peak field entering and the mean value of the signal exiting the head. A virtual channel is similar to a regular MEG channel except that it is tuned to detect activity of focal, desired brain region (Gross and Ioannides, 1999). In general the reduced dimension of virtual channel is less sensitive to noise that is uncorrelated among channels. This is due to the linear transformation, which is essentially a weighted averaging of the original channel signals, so that uncorrelated noise is reduced. For details of the definition of virtual sensor and its applications see Liu et al (1998).

Two virtual channels were defined; one for the SEF measurements sampled at 4165 Hz, and one for the phantom data sampled at 4165 Hz (Fig. 3). For the SEFs, the virtual channel was defined from the contour map of one-subject's high-band HFO showing the iso-magnetic field during the M20 peak. The field maps for left median nerve stimulation showed a dipolar pattern over the right somatosensory area at 22.4 ms. A similar single dipolar pattern was also seen for the phantom data, when the PhS1 dipole was activated. The virtual channel was defined from the field map during the peak of the delivered pulse.

2.2.5. Co-registration of MEG and MRI

The phantom was scanned using a 1.5 T MRI Scanner (Model ExcelArt, Toshiba Medical Systems). Fiducial radio-opaque washers were placed on the phantom on three out of the four coil mounting positions (equivalent to the nasion, left, and right ears) (see Fig. 1A). A volume acquisition scan was performed with T1 weighted images. Three standard magnetic fiducial coils were then placed on the phantom mounting positions. The MRI/MEG co-registration was calculated by using the head localisation system. The volunteers' heads were scanned with the same MRI system. For the SEFs experiment, three head localisation coils were attached on the fiduciary points: one on the nasion and two on the right and left preauricular points. Two extra coils were attached to the right and left forehead, and collected together with the three fiduciary points. The surface of the head and face, with all five coils, was digitalized using a 3D non-contact laser scanner (VIVID 700, Konica Minolta, Japan) and a 3D digitizer (Polhemus, 3Space/Fastrak, USA). In addition, the relative positions of additional coils were determined by activating them one-by-one and measuring with

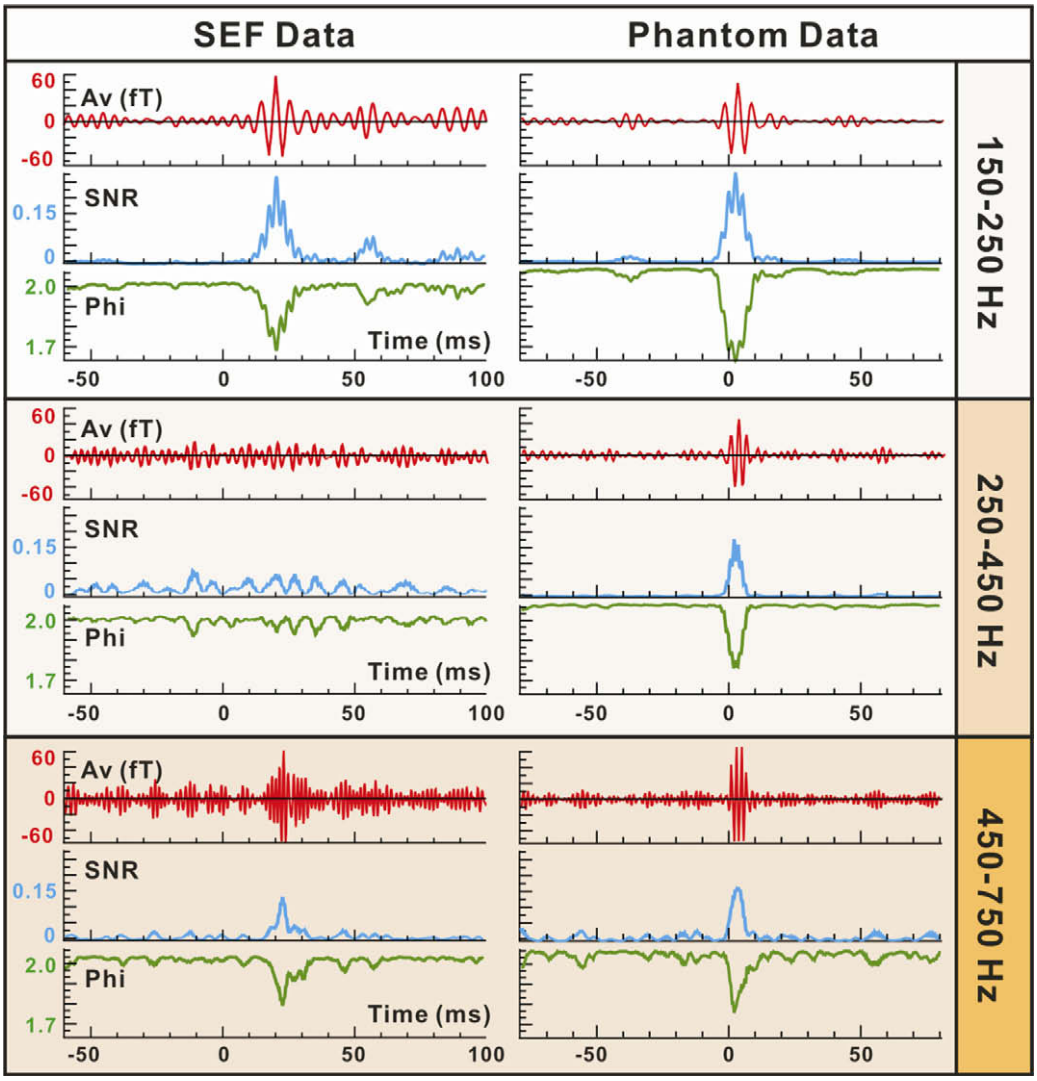

Fig. 3. Comparison of band passed virtual channel traces derived from 120 trials recorded with high-sampling rate (4165 Hz). The SEF (left wrist stimulation) data are on the left and the data for the phantom on the right. Results in three frequency bands are displayed, 150–250 Hz (top-row), 250–450 Hz (middle-row) and 450–750 Hz (bottom-row). For each band three measures of the signal are shown, the average (red), SNR (blue) and ITS (green). SEF data from −60 to 100 ms, phantom from −80 to 80 ms. SEF changes seen at time of M20, phantom at time of 2 ms pulse. Note that no measure shows high values in the 250–450 Hz band for SEF data. The phantom data correspond to the dataset of 5 μA.

the MEG system. The combination of head surface details provided by Polhemus, VIVID camera and additional coils on the head was used to reconstruct the subjects' head shape as accurately as possible. The two extra coils were then removed. An in-house procedure was used to coregister the digitized points of the head (including the fiduciary coils) to the MRI and the brain. It uses the digitized head shape, with the information from the coils (fiduciary and extra) (Hironaga and Ioannides, 2002). The three fiduciary coils were activated at the beginning and the end of each experimental run. Analysis solutions were always referred to the source space defined by the subject's brain.

2.3. Data modeling

For the analysis at the level of sensors, we used two standard measures of reproducibility across trials in addition to the averaged signal; the signal-noise-ratio (SNR) and the intertrial synchronization index (ITS) (Laskaris and Ioannides, 2001). Each of these measures was computed for a moving window providing a time-dependent quantification of the signal content of the ensemble of single trials (STs).

The average signal ($\bar{X}$), the noise power (NP), the signal power (SP), and the SNR for this window are defined as below (Laskaris and Ioannides, 2001):

$$\bar{X} = \frac{\sum_{i=1}^{N} X_i(t,p)}{N},\quad NP = \frac{\sum_{i=1}^{N} \|\bar{X} - X_i(t,p)\|_{L_2}^2}{p(N-1)},$$
$$SP = \frac{1}{p}\|\bar{X}\|_{L_2}^2 - \frac{1}{N}NP,\quad SNR = \frac{SP}{NP}$$

The $\bar{X}$ is the ensemble average of N ST patterns, each with p samples and time between samples t. The NP is the ensemble average of ST deviations from $\bar{X}$, computed with the L_2 norm. The SP is the noise-corrected L_2 norm of $\bar{X}$. The SNR can be thought of as the ratio of the "energy" in the reproducible part of the signal divided by the "energy" of the residual signal across STs. The ITS provides a complementary measure to SNR, testing the changes in the phase of the ST signal. It is defined as:

$$ITS = \frac{1}{N(N-1)} \sum_{i=1}^{N} \sum_{j \neq i}^{N} \left\| \frac{X_i(t,p)}{\|X_i(t,p)\|} - \frac{X_j(t,p)}{\|X_j(t,p)\|} \right\|$$

For pattern segments with no resemblance in the different STs, the ITS is about two, and it progressively approaches zero as the STs become more similar. In the limit with STs with identical response patterns, ITS becomes zero. Note that because of the normalization with the norm of the segment, ITS is not sensitive to the overall strength of the ST response, but only to the shape. ITS therefore measures the effectiveness of 'phase resetting' in the evoked response across trials.

MEG data sampled at 2083 Hz were processed using the latest version (Version 5.4.0 – linux-20061212) of the CTF (VSM MedTech Ltd, BC, Canada) software for ECD, SAM and MUSIC and in-house software for MFT. The use of standard commercially available software was justified as it is commonly used by the MEG community. The data were initially filtered in the low-band. Two variants of the sphere model were used to describe the conductivity. A single sphere (SS) model, in its standard form, was used with its center selected to coincide with the best fitting sphere of the phantom or inside surface of the skull. The second model used a different local sphere for each MEG sensor (multiple local spheres model, MLS), selected to fit the curvature of the phantom or inner skull surface just below the sensor. The true position of the dipoles was determined from the MRI. The MRI distortion was found to be negligible, as it was verified by the phantom's physical dimensions. A separate MRI was obtained for each single or multiple dipole configuration. The distances between the true and estimated dipole positions were tabulated for each source localisation method, volume conductor model and dipole current. In this paper, we name a localisation accuracy of 0–5 mm as very good, 6–10 mm good, 11–15 mm satisfactory, 16–25 mm poor, and 26–40 mm as very poor. A one-way ANOVA with post hoc *t*-tests was performed to examine significant differences of the means for the different methods.

2.3.1. ECD

The ECD model assumes that the MEG signal is generated by one or more focal sources. Each source is then described by an infinitesimally small line current element and the task is to find the location, direction and moment of each ECD (Hamalainen et al., 1993). The ECD sources, in both phantom and SEF data, were estimated by a normalized least square fit algorithm. For the phantom data, averages of six, 120, and 360 trials were calculated. For the SEFs, data averages of 120 trials were calculated. STs phantom data were also analysed. The estimated location was taken to be the center of gravity of the STs dipole estimates. The ECD fit for the phantom was analysed at the peak of stimulation, with dipoles seeded at a distance of 3 cm from the true dipole location. The ECD was also calculated by using a subset of sensors in order to examine how this widely used methodological approach affects the MEG localisation accuracy. The isofield contours guided the visual selection of the subset of sensors; the selection ensured the inclusion of the dominant features of the topography (Salmelin and Hari, 1994). Approximately 40–60 sensors were used in each subset for all runs. The ECD fit for the SEF data was analysed at the peak of the low-band HFO component where this was seen in the averaged signal. The dipole was seeded at a distance of 3 cm away from the area S1, contralateral to the stimulated wrist.

2.3.2. SAM

SAM is a beamformer method, with a spatial filter designed to detect signals from a specified location and attenuate signals from all other locations (Robinson and Vrba, 1998; Taniguchi et al., 2000). The dual-state imaging approach was used here. We calculated the source power difference between the active and control intervals for each 2 mm cubic volume element within the conducting volumes. The source power difference between the two intervals was normalized with respect to the noise variance to give a pseudo *t*-statistic (Robinson and Vrba, 1998). We computed the true *t*-statistic value from the multiple-trial SAM images of active and passive activity,

$$T_\theta = \frac{\overline{{}^{(a)}\hat{Q}_\theta^2} - \overline{{}^{(b)}\hat{Q}_\theta^2}}{\sqrt{\sigma^2/N}}$$

where σ^2 is the pooled variance and N the total number of instances of both the active and control events (Vrba and Robinson, 2001). Then, the p statistical value was estimated taking into account the degrees of freedom for each experimental design. Sources with a $p < 0.01$ were assumed as statistically significant. For phantom data, the active and the passive intervals were: 0–5 ms and −5–0 ms respectively. SAM was applied to the unaveraged phantom data with six, 120, and 360 trials, as well as to the unaveraged data of SEFs. For SEFs data, the active and the passive intervals were: 10–30 ms and −30 to −10 ms respectively. Time intervals with different lengths were used for the phantom and SEF data. The more limited time range used in SAM analysis for the estimation of the covariance matrix makes statistical significance harder to get. This selection was made assuming that the phantom dipolar sources are slightly easier to be localised than the real neural sources in human data.

2.3.3. MUSIC

The MUSIC method (Mosher et al., 1992) estimates a signal subspace from the recorded MEG data using a singular value decomposition. The MUSIC algorithm then scans a single dipole model throughout a three-dimensional head volume and for each position estimates the projection of the model MEG signal onto the signal subspace. MUSIC analysis utilized the corresponding covariance matrices that had already been generated for the SAM analyses. The eigenvalue spectrum was obtained from the covariance matrices, following eigendecomposition. First, the eigenvectors for the noise subspace were identified and eliminated. The dipole model was scanned with 2 mm steps and the method was applied to the unaveraged phantom data with six, 120, and 360 trials, as well as the SEF data. The same time intervals as for SAM analysis were used. The strongest source localised by the algorithm was assumed as significant for each separate dataset.

2.3.4. MFT

MFT relies on a non-linear algorithm with optimal properties for tomographic analysis of the MEG signal (Ioannides et al., 1990; Taylor et al., 1999). MFT computes the three-dimensional distribution of primary current density vectors throughout the brain at each timeslice (in our case every 0.4 ms). For phantom data, we applied MFT analysis to the averages of six, 120, and 360 trials and to STs MEG signals. For SEF data, MFT analysis was applied to the MEG signal for the averages of 120 trials and to STs MEG signals. A time window for determining the baseline distribution was selected from the pre-stimulus period (phantom data: −1.8 to −1 ms; SEFs: −30 to −10 ms). The windows for an 'active' distribution had identical lengths as the ones for the baseline and they were stepped in the post-stimulus period from 0 to 3.4 ms (step 0.4 ms) for phantom data, and from 0 to 100 ms (step 3.2 ms) for the SEF data. Statistical comparisons between pre- and post-stimulus periods of STs MFT solutions were calculated using student's *t*-tests to generate a statistical parametric map (SPM) for each run. The procedures used were identical to the ones described in Poghosyan and Ioannides (2007).

2.3.5. Probabilistic cytoarchitectonic maps

The use of probability cytoarchitectonic maps (Amunts and Zilles, 2001) provides a powerful tool for the analysis of structure-function relationships in the human brain. In order to identify

the cytoarchitectonic area of the HFO generators, we superimposed the localisation estimates of the SEFs on the probability cytoarchitectonic maps for each one of the four different source localisation methods. This was done by using the public domain "Anatomy Toolbox" software (v1.5) (Eickhoff et al., 2005, 2006, 2007).

3. Results

3.1. SEF averages

HFO could be clearly seen in the filtered averaged SEF signal from the virtual channel for two frequency bands, the low-band and the high-band, using only 120 trials. The low-band was seen using both the sampling rate of 2083 Hz and the high rate of 4156 Hz. The high-band HFO were only detected with the 4156 Hz. This was due to filter settings that cut the frequencies above 600 Hz for the MEG data sampled at 2083 Hz. No clear HFO was seen in the medium-band. The left column in Fig. 3 shows the averaged SEF data filtered in the three different frequency bands. The low-band and the high-band HFO have almost the same signal amplitude (red trace), although the SNR of the low-band is twice as high (Fig. 3). The green trace shows the ITS for both frequencies.

3.2. Phantom data

3.2.1. Averages

An excellent representation of the somatosensory-evoked HFO signal at the virtual channel level was generated (Figs. 2 and 3), by using the spheroid phantom and activating the superficial dipolar source PhS1 (see Fig. 1) with simple triangular pulses. The artificial signal was derived after following exactly the same hardware and software filtering procedure as during the processing of SEF data. The moment of the phantom's activated superficial source was adjusted so that the generated virtual channel signal was similar in amplitude to the virtual channel signal of the HFO in the subject data (see Fig. 3). The HFO roughly corresponded to dipole currents of 5 μA. Both SNR and ITS amplitudes were similar to the SEF analysis. A response from the phantom signal was seen in all three frequency bands. This suggests that the absence of medium-band in the SEF data is likely to be due to the absence of a cerebral generator at those frequencies.

3.2.2. Single source activation

The localisation accuracy of each source localisation method was tested using both SS and MLS (Fig. 4) models, when a single phantom source was activated in one of the four locations (PhS1, PhS2, PhS3, and PhS4) (see Fig. 1B). SAM, MUSIC, MFT and ECD on averages (Av-ECD) localised the most superficial dipole (PhS1) at dipole currents as low as 3–5 μA, with a very good localisation accuracy of 2–3 mm using the 360 trials data and 151 sensors (Fig. 4). The differences in localisation accuracy between these four methods was only a few millimeters ($F(3,76) = 2.72$, $p = 0.3$). In general, the MLS model presented slightly better localisation accuracy than the SS model (Supplementary Figure S1), with the most noticeable improvement for SAM. For the MLS model, MFT, MUSIC and SAM maintained very good localisation accuracy (about 2 mm for MFT and MUSIC, and 4 mm for SAM) even for the low dipole currents of 3 μA (Fig. 4). For the lowest dipole current, the best localisation accuracy (1.9 mm) was obtained from an ECD fit calculated on averaged data for the SS model (see Supplementary Figure S1). For the other methods, the lowest dipole current for which very good localisation accuracy was obtained was 2 μA for MUSIC and MFT, 4 μA for SAM, and 20 μA for ECD on STs data. ECD with a subset of sensors did not improve the localisation accuracy of dipole fitting (see Supplementary Figure S2).

The ECD fit applied to the STs data by using either all sensors or a subset of sensors failed to fit the data for dipole currents below 10 μA that correspond to the weak signal of HFO for the superficial dipole PhS1. These two ECD models will not be further discussed, since their performance was even worse for the more difficult cases that follow, but an interested reader can inspect the results in the Supplementary Figure S2.

The performance of the source localisation methods varied for the sources away from the surface and/or close to sharp discontinuities. For deep dipoles the use of the MLS model led to big improvements in localisation accuracy for the ECD and SAM methods. We will emphasize the results using the MLS model, i.e. Fig. 4, but the interested reader can always compare the results using MLS and SS model by contrasting the corresponding curves in Fig. 4 and Supplementary Figure S1. For source PhS2, SAM and MFT presented better localisation accuracy compared to ECD and MUSIC for the MLS model (Fig. 4). The localisation accuracy of MFT was slightly higher compared to SAM. In terms of sensitivity, the lowest dipole currents for which statistically significant results were obtained for SAM and MFT were respectively 5 and 3 μA. The use of MLS model improved the localisation accuracy for SAM by a factor of two.

For the dipole position PhS3, the best localisation accuracy was obtained by using Av-ECD and MFT (Fig. 4). Av-ECD showed good localisation accuracy (5.8 mm) at dipole currents of 2 μA, while MFT (5.5 mm) at 3 μA. For this dipole position, all methods produced substantially better results using the MLS than the SS model (see Figs. 4 and Supplementary Figure S1).

Poor localisation accuracy was expected for the deepest source, PhS4. All methods, except MFT and Av-ECD, applied to average data, generally failed to localise this source accurately, even for the highest dipole currents (Fig. 4). Av-ECD showed a good localisation accuracy of 8 mm for dipole currents of 6 μA (Fig. 4), while SAM's accuracy for the same dipole current was satisfactory. However, despite the accuracy no statistically significant results were obtained with SAM analysis for any dipole current. MFT applied to averaged data maintained very good localisation accuracy even for very weak currents (1–4 μA). However, the SPM analysis of STs MFT solutions produced statistically significant results only for the three strongest currents (see Fig. 4). The localisation accuracy of MUSIC was generally poor. Using the MLS model however, the localisation results of MUSIC improved dramatically as the dipole current increased above 15 μA, producing a very good localisation accuracy of 1.5 mm for the strongest dipole 20 μA (Fig. 4).

In summary as one would expect, the ECD model failed when applied to STs data (except for very strong superficial sources). In contrast, the Av-ECD model (360 trials) using all sensors produced very good results. All methods gave very good localisation accuracy for the superficial source, even by using the SS model. For the sources corresponding to subcortical areas (PhS2 and PhS3), Av-ECD and MFT maintained good localisation accuracy (~5 mm) throughout. For the two deepest sources, the ECD approach (based on averaged data) generally outperformed SAM and MUSIC. This could be attributed to the fact that only a single dipolar source was active with no jitter between trials. If only a single deep source is present then averaging will perform well and it will reduce noise leaving a dipolar signal pattern that the single dipole model can match to. Both MUSIC and SAM rely on dipolar patterns in single trials repeating consistently to be picked up. For deep and especially weak sources the ever-present noise does not allow such patterns to survive in many single trials. This may explain why SAM and MUSIC performed worst than ECD on averages for deep sources in our phantom data. All methods, except MFT of averages, generally failed to localise accurately the deepest source. MFT

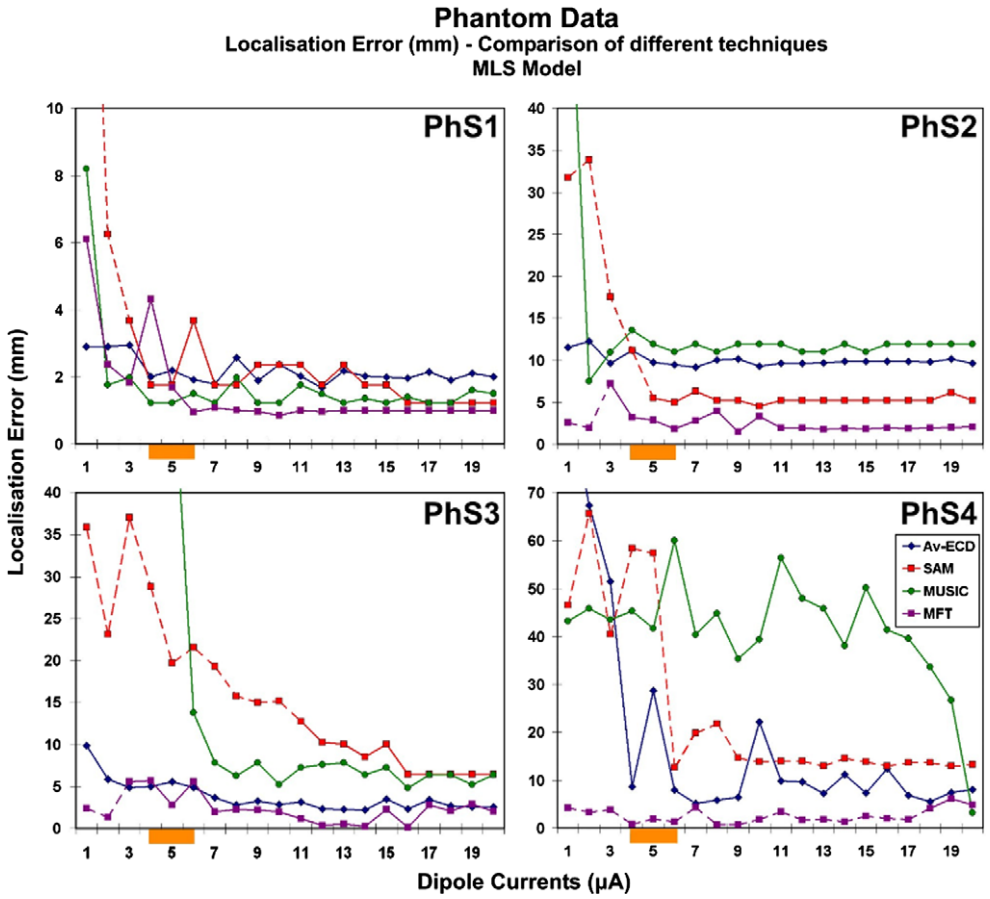

Fig. 4. The LE (in mm) versus the dipole current (in μA) using the MLS model for four different dipole locations (PhS1, PhS2, PhS3, and PhS4). The results were obtained from datasets with 360 trials. Dashed lines, values with no significant *t*-values for SAM. For MFT, dashed lines represent LE of MFT derived from the average signal (used when MFT analysis of STs data produced no significant *t*-values). Orange bars under the *x*-axis – HFO signal amplitude.

solution of the average data (360 trials) maintained a very good accuracy for the 'thalamic' source PhS4 even for the lowest dipole currents.

3.2.3. Number of trials

In order to test how the localisation accuracy of MEG is affected by the number of trials, phantom datasets with different trial numbers (six, 120, and 360 trials) were used. For the superficial dipole position PhS1 and weak currents (5 μA), all source localisation methods maintained a good localisation even when very few (six) trials were used. However, an increase in the number of trials from six to 360 affected significantly the localisation accuracy, improving it to approximately half the localisation error (LE). The worst performance for six trials was provided by MUSIC and Av-ECD (5.8 mm) (Fig. 5, col. 1). Decrease in trial number from 360 to six, tripled their LE, while it did not affect the localisation accuracy of the other methods.

Similar results were derived for the dipole PhS2. The localisation accuracy for six trials was very poor for SAM and MUSIC at 5 μA (Fig. 5, col. PhS2) and for SAM with 120 trials. MFT and Av-ECD showed consistently good localisation accuracy for PhS2 as did the other methods for higher dipole currents and trials. For the dipole PhS3 (Fig. 5, col. 3), all source localisation methods were significantly affected by the number of trials and dipole currents. SAM performed worst across all currents and trials, with MUSIC next. For the deepest dipole PhS4 (Fig. 5, col. 4), most methods produced high LE especially for the two datasets with low trial numbers. Overall MFT showed low LE for 360 trials independent of dipole current, while Av-ECD presented good localisation accuracy only for the strongest currents of 15 and 20 μA. Counterintuitive results in Fig. 5 presenting an increase of LE with increasing dipole currents or increasing number of trials are very likely due to different levels of system noise between the different datasets.

3.2.4. Simultaneously active sources

When two dipoles were simultaneously active (PhS1 and PhS3), ECD and MFT analysis on averaged data gave the best results (Table 1). STs ECD calculations failed to localise either of the dipolar sources (data not shown). Simultaneous activation of other sources revealed similar results. The MLS model presented better results than the SS model for all methods (data not shown). As expected, the total LE was much higher for simultaneous activation of two sources than the sum of errors when each source was activated separately. For SAM, the results did not reach significance for either location (data not shown), but rather surprisingly the deep dipolar source PhS3 was localised by SAM better than the more superficial one PhS1 (Table 1).

When three dipoles were activated simultaneously, SAM and MUSIC identified a generator reasonably close to the superficial source, but these two methods failed to detect a source within 30 mm of the other two (Table 1). More worrying, SAM produced a statistically significant ($p < 0.01$) localisation 33.5 mm away from the nearest generator (source PhS3). As expected given the results for single sources, ECD applied to STs failed to localise any one of the three sources. All sources were detected and localised with a good accuracy, when the averaged data were used with either

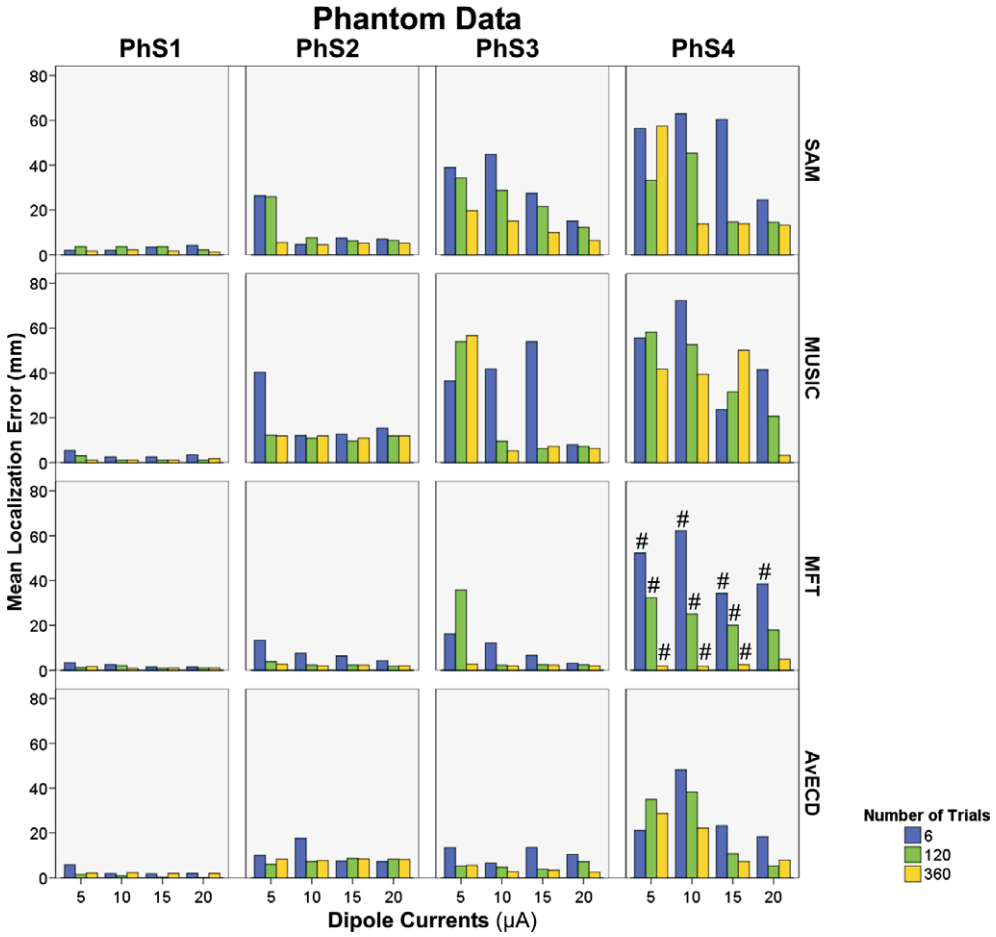

Fig. 5. The LE (in mm) estimated for all dipoles and different source localisation methods using different runs with different number of trials (six, 120, and 360 trials) and with MLS model. The symbol # indicates the LE obtained by MFT applied to averaged data.

ECD or MFT (Table 1). The MLS model presented much better results than the SS model for all source localisation methods (data are shown in Table 1 only for MLS model).

3.3. The localisation of HFOs generators

Fig. 6a presents the localisation results of the low-band HFO for subject 2 and all source localisation methods. Similar results were derived for the other subject. Fig. 6b presents the localisation results of phantom data that have the same amplitude with low-band HFO at the virtual channel level. The low-band HFO generator was localised in the contralateral Broadmann area 3b according to the probabilistic cytoarchitectonic maps (Fig. 7) by using all source localisation methods for both subjects and stimulation of the left and right wrists.

Table 1
The mean LE (in mm) of different methods localising two (2DS), and three (3DS) simultaneously active dipoles by using the MLS model. In the brain, two dipoles would be roughly located by right SMA, and right hippocampus, third dipole in area behind eyes. Estimated dipoles positions, obtained using different source localisation methods. Note when three dipoles activated simultaneously, SAM and MUSIC fail to detect source behind eyes.

	DS	Av-ECD	SAM	MUSIC	MFT
2DS	PhS1	2.6	14.4	12.3	5.9
	PhS3	7.5	6.8	22.5	4.7
3DS	PhS1	10.8	4.9	10.5	4.2
	PhS2	7.3	Failure	Failure	9.7
	PhS3	5.2	33.5	33.3	7.9

4. Discussion

This paper set out to study the localisation accuracy of MEG for weak, transient, neural sources, such as the HFO, with the commonly used source localisation methods. To do this the paper looked first at sensory evoked responses from median nerve stimulation and then using the HFO amplitude as a guide examined realistic phantom data. An artificial MEG signal was generated by activating simple dipolar sources in different but precisely determined locations inside the phantom.

4.1. Sensory evoked response – number of trials

A very large number of trials (6,000–20,000 trials) is usually recorded and averaged offline to detect and characterise HFO (Gobbelé et al, 2004; Hashimoto et al., 1999; Haueisen et al., 2000, 2001). It is clear from the analysis of the filtered SEF data that fewer trials (a hundred or so) in the average signal are able to show the presence of HFO superimposed on the averaged M20 somatosensory-evoked response (Fig. 3). This high frequency oscillatory activity was distributed in two distinct frequency bands: 150–250 Hz and 450–750 Hz (Fig. 3). Our findings are in agreement with previous studies in both humans (Haueisen et al., 2001) and animals (Jones et al., 2000) showing two distinct types of fast oscillations in the somatosensory cortex. The two frequency

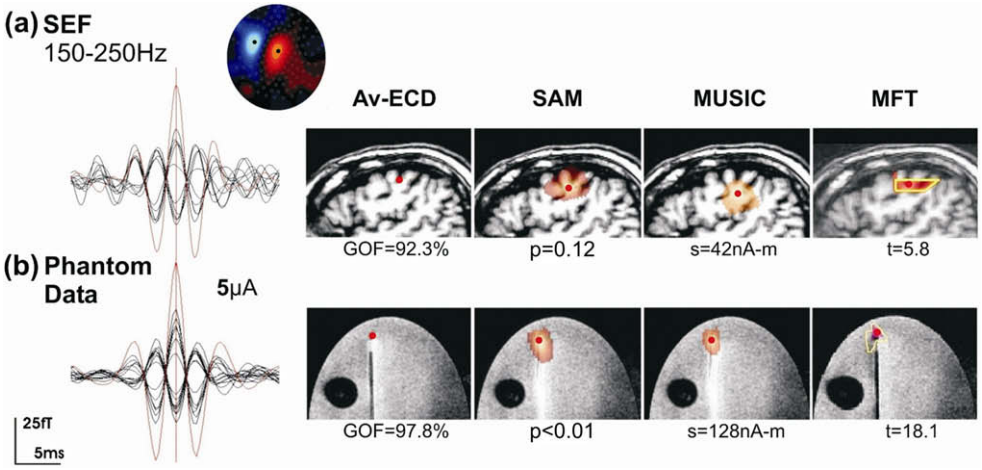

Fig. 6. (a) Human SEF (right wrist stimulation) of low-band HFO signals and (b) phantom data with similar signal amplitude. Low-band HFO signal corresponds to phantom data with a dipole current of 5 μA. Contour map shows iso-magnetic fields during M20 peak for low-band HFO, a single dipolar pattern over right somatosensory area, in black MEG sensors used in the virtual channel. Black trace butterfly plots show MEG signals of individual sensors. Red curves show output of the virtual channel. The right panel displays the results for all source localisation methods for the SEF (top) and phantom data (bottom). In each case the results are shown with the background anatomy of the subject's or phantom's MRI. The estimated measures of the quality of fit are printed below the figurine for each method (Goodness of Fit (GOF) for ECD, *t*-value for SAM, estimated dipole moment for MUSIC, and *t*-value of SPM significance for MFT).

bands gave the same signal amplitude on the average signal of the virtual channel. The SNR of the low-band was however almost twice that of the SNR for the high-band. It thus appears that the HFO signals may be generated by more than one generator with the slowest generator being the dominant one. We were not able to detect the high-band HFO, with our lower sampling rate and a cut-off at 600 Hz. With the higher sampling rate just above 4 KHz the high-band HFO were detected, and the critical factor was that the frequencies above 600 Hz were not eliminated.

4.2. Use of phantom to generate HFO

Based on these results and using the spheroid phantom model of the brain and skull, artificial MEG signals that were very similar to the HFO were successfully generated (see Fig. 3). A single triangular pulse with 2 ms duration was used in conjunction with system noise. Although the use of oscillatory driving signal for our dipolar sources will provide a more straightforward simulation of HFO generators, this approach will impose a very specific morphology for HFO generators in single trials. The morphology of HFO generators in single-trials level is so far unknown (Hashimoto, 2001), since HFO can be recorded either invasively or non-invasively after a very specific methodological approach namely filtering in a specific frequency band and averaging afterwards. Furthermore, our analysis will be biased towards a very specific frequency. The human HFO have a wide range of frequencies peaking around 200 and 600 Hz (Haueisen et al., 2001), rather than a very specific frequency peak in the spectrum domain.

4.3. Localisation of phantom sources

We examined the accuracy with which weak transient sources from our phantom -able to generate an artificial MEG signal similar to the human HFO after processing- could be localised with currently available and commonly used source localisation methods. The MEG signal from median nerve stimulation gave a range of moments for the implanted dipoles that covered the physiological range of somatosensory-evoked HFO. This corresponded to a phantom superficial source with 5 μA dipole current (Fig. 3). The range of dipoles moments based on the HFO values was extended to generate signals more than three times smaller (1 μA) and three times larger than the HFO amplitude (15 μA). The study of lower

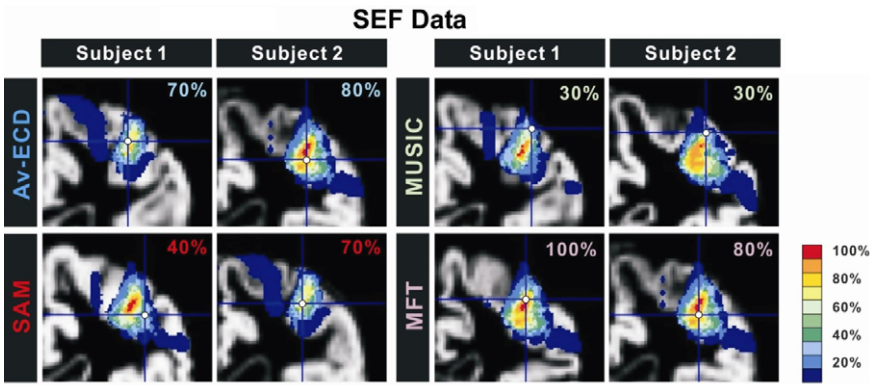

Fig. 7. Correspondence of estimated generators to cytoarchitectonic areas for two subjects, subject 1 on the left and subject 2 on the right. Rows show the results for source localisation methods for left wrist stimulation. The source estimates are over-plotted on each subject's MRI and the probabilistic cytoarchitectonic map for Broadmann area 3b.

(1–3 μA) and higher values (15–20 μA) ensures that the range covers what might be the strength of high frequency activity that seems to precede strong pathological bursts in epilepsy (Bragin et al., 2002) and the strong interital signals recorded next.

Our phantom source PhS1 was located at a superficial position and is representative in terms of localisation difficulty of sources in cortical area S1 (Fig. 1B). Its localisation thus represents the localisation accuracy of MEG for HFO assuming one generator near the M20 source in Broadmann area 3b (Curio et al., 1994, 1997; Hashimoto et al., 1996, 1999; Ozaki et al., 1998). Overall for this superficial source, a very good localisation accuracy was obtained with all methods even when only six trials were included in the analysis (Fig. 5). All source localisation methods produced similar results, with the only exception of ECD applied to STs (see Supplementary Figure S2). Even when a subset of sensors over the relevant region was used (Liljestrom et al., 2005), ECD failed to localise accurately the active dipole from STs MEG data.

ECD using a subset of sensors has been used with apparent success in the localisation of spontaneous brain rhythms generators in the time and frequency domains (Salenius et al., 1997; Salmelin and Sams, 2002; Salmelin et al., 2000). One assumes that the underlying source currents can be represented by a single ECD. Although in some cases (e.g. when one is interested in the sensorimotor rhythms) the selection of subsets of sensors is fairly straightforward (Liljestrom et al., 2005), it generally becomes quite difficult when the spatial and spectral distribution differs from the normal pattern, and requires that a highly experienced researcher generates the models by trial and error. Since no averaging is applied, the locations of the dipoles are highly affected by noise. In our study, ECD using a subset of sensors gave higher LE for the superficial phantom source (PhS1) in comparison with the use of the whole array of sensors, while it did not improve the localisation of the other two sources (PhS2 and PhS3). Our results are in accordance with previous studies (Vrba et al., 1999) showing that the use of a subset of sensors in ECD analysis reduces the localisation accuracy of MEG.

The very good localisation accuracy of methods even when few trials were used provides support for arguments against the common practice of averaging large numbers of trials for superficial generators (Laskaris et al., 2003; Liu and Ioannides, 1996; Makeig et al., 2002). Based on the findings revealed from the phantom data analysis, we can be confident that the low-band HFO can be accurately localised assuming a superficial source at the level of S1. All methods localised the low-band HFO generator in the contralateral Broadmann area 3b (Fig. 6). The anatomical location of this generator was described objectively using the probabilistic cytoarchitectonic maps (Fig. 7).

4.4. Deep single source location

We also used deeper dipolar sources placed in the phantom corresponding to subcortical and thalamic regions, since there is evidence that HFO in humans are generated by sources that are not restricted to the cortex, but are also located at subcortical and even subthalamic sites (Gobbelé et al, 2004). As was expected, the deeper sources were localised less accurately. The source located behind the eyes (PhS2) was localised with very good accuracy (for dipole current of 5 μA, the LE for MFT was 2.8 mm, while for SAM was 5.5 mm). For this source, the high-dimensional source localisation methods, such as MFT and SAM, produced better results than the ECD-based models, such as ECD fit and MUSIC (Fig. 4). This may be attributed to the position of this source. The PhS2 dipole was placed close to the inner plastic surfaces that resembled the eye sockets. The electrical current flow generated by this source in the nearby medium would change rapidly as the current is channeled along the inner surface of the "eye socket". So the effective source will have a finite extent and shape. This may be better described and localised by distributed source methods than by dipole methods which work better for point-like sources (Phillips et al., 1997). The good localisation accuracy of SAM suggests that the spatial filter placed at the actual source location can still perform reasonably well. However, since SAM also uses sequentially a dipole at each region-of-interest as its source model, it is not entirely clear why SAM worked well for this dipolar source.

The PhS3 source at "hippocampus" was localised with a localisation accuracy of ~5 mm by using either Av-ECD or MFT with STs data and all dipole currents, while the results were slightly worse (~10 mm) for MUSIC. The localisation results were poor for the deepest source PhS4 representing sources at thalamic and hypothalamic level. This is not surprising since MEG becomes progressively blind on approaching the center of the head. Only MFT showed good results for the SS model for all dipole currents and trial numbers. For the MLS model MFT remained good. MUSIC achieved 2 mm accuracy for the strongest dipole current and 360 trials. It was possible to localise deep "thalamic" sources with a satisfactory accuracy (1 cm or better) provided that sufficient trials were available for improving the SNR of the MEG signal.

4.5. Localisation of multiple sources

It had been assumed that multiple sources activated almost in parallel are responsible for HFO brain activity (Gobbelé et al., 2004). To test the localisation accuracy of MEG for multiple simultaneously active sources, the phantom dipoles were driven in synchrony. The activation of multiple sources showed bigger differences between the source localisation methods. SAM, MUSIC, and MFT make no assumptions about the number of active sources. ECD requires a priori knowledge about general regions of interest and the number of sources. MFT and Av-ECD showed the best results for two (mean LE: 5.3 mm, and 5 mm respectively), and three active dipoles (mean LE: 7.3 mm, and 7.8 mm respectively). They localised all sources with a good accuracy. SAM and MUSIC failed to localise the PhS2 source behind the eyes. SAM's failure to detect this source can be explained by its known limitation to suppress spatially separate, yet temporally covariant sources (Brookes et al., 2007). SAM produced a very good localisation for the superficial source, PhS1, when three sources were simultaneously active, but failed to identify the other two. The poor localisation accuracy of MUSIC and SAM for multiple sources was expected when the sources were synchronous. The results do show that even in these cases erroneous solutions with high statistical significance can be produced. It thus underscores the need for caution and careful selection of source localisation method to use when the cerebral activity being studied is likely to have several synchronous generators. We nevertheless note that our artificial sources were perfectly coherent, an unlikely scenario for distinct brain regions separated by several centimeters. In the case of less synchronous generators, SAM may be more effective in the accurate localisation of multiple synchronous sources.

4.6. Accuracy of the volume conductor models

The localisation accuracy of MEG depends on errors in the volume conductor model of the head (i.e. the forward model). A good estimate of skull shape is a prerequisite for accurate localization (Huiskamp et al., 1999). Realistic head models provide a potentially accurate but computationally costly solution (Darvas et al., 2004). The spherical model is the simplest approach to the forward problem. All that is required to compute the forward problem is the center of the sphere (estimated by fitting to a sphere the inner surface of the skull) and the location and orientation of the sensors

(Sarvas, 1987). A better model is obtained by replacing the simple SS model with a different choice for the sphere center for each MEG sensor, obtained by fitting the local inner skull surface below each sensor (Huang et al., 1999).

In earlier studies, two models have been used for the HFO localisation, either the simple SS model (Gobbelé et al, 1998; Hashimoto et al., 1999) or a four-shell spherical head model (Gobbelé et al, 2004). In this paper, the localisation accuracy of MEG was tested by using both the SS and MLS model. For the superficial dipole, the MLS model presented slightly better results for SAM and MUSIC, but did not change the results from either ECD or MFT. This finding agrees with previous phantom studies (Leahy et al., 1998), which reported little difference in LE (<1 mm) between different head geometry models, for dipoles positioned at superficial locations. The head model choice altered the localisation of deeper sources. For deep sources corresponding to the thalamus, the SS model is inadequate. Even small departures from a sphere made an important difference with large improvement being obtained by using an approximate model, provided symmetry is broken in the right direction (Fieseler et al., 1996). The MLS model achieves this correct approximate break of symmetry. It seems to provide similar accuracy with the Boundary Element Method (BEM) (Hamalainen et al., 1993) in an economical and practical way (Huang et al., 1999), and also similar or even better results than the volume-based Finite Element Method (FEM) for superficial sources (Uitert and Johnson, 2002).

4.7. Study limitations

Despite our efforts to be comprehensive, our study has some limitations that should be stated. It is important to emphasize that with the present study, we did not demonstrate that MEG can localise deep sources. To do so would require identifying deep generators in the real MEG data. The analysis of the phantom data showed that the results for some methods could be very different when a single or multiple sources are active simultaneously. It was therefore impossible to make a fair comparison of the different methods without a priori knowledge of the single trial activation time course of generators at different levels (e.g. cortex, thalamus and brainstem). A separate study dedicated to this point is in progress and the results will be reported in a separate paper. The phantom data reported here suggest that MEG might be able to localise deep sources and one of the prerequisites is that a large number of trials is necessary in order to increase the SNR, and an appropriate source analysis method must be used. Our spheroid phantom provides insights under realistic measurement conditions that are not easy to emulate with computer stimulations. However, the shape and conductivity details of a real head are far more complex than those of our phantom. The effort for more realism could be advanced with the use a human skull phantom with multiple dipoles implanted within the whole volume, which are activated independently in a random order within the physiological range of source strengths. Since this was technically impossible with the available instrumentation in our lab, it remains to be shown in future studies. A more realistic approach should also take into account the background brain activity unrelated to the HFO that can confound the localisation accuracy of the inverse techniques. To simulate this effect, spontaneous brain activity recorded separately from a human subject should be added to the recorded phantom data.

5. Conclusion

Our phantom study provides strong evidence that MEG has a very good localisation accuracy of 2–3 mm for weak, transient superficial sources, even when a small number of trials and/or the simple SS model are used. The localization of the slower HFO activity (~200 Hz) provides an example where such capability is useful. Each of the source localisation methods that we have reviewed, even when the simple SS model and a small number of trials were used, localised the slow HFO activity in Brodmann area 3b using the standard tools for cytoarchitectonic assignment (Eickhoff et al., 2005, 2006, 2007). The HFO activity around 600 Hz can clearly be observed at the level of the virtual channel signal, sampling at 4 KHz, by using only a hundred trials. Where and how best the generators can be localized remains to be shown by teams with hardware that can record at 4 KHz, or higher frequencies, for all MEG sensors. The phantom data has clearly shown that weak, transient sources located in subcortical areas such as putamen, fusiform gyrus, hippocampus and amygdala can be localised with good accuracy (~5 mm) provided that an appropriate method is used. Our results for activity generated by deep sources in our phantom suggest that it is necessary to collect more trials increasing the SNR of MEG signals to localise deeper 'thalamic' sources (within about 2 cm from the center of the head). Accurate localization of such deep sources demands realistic head models and source localisation methods, like MFT, that are effective in the presence of multiple distributed sources.

Acknowledgements

We thank all the staff of the HBD lab and especially Mr. Kenji Haruhana. We also thank Prof. Christoph Braun for helpful suggestions in the final revision of the manuscript.

Appendix A. Supplementary data

Supplementary data associated with this article can be found, in the online version, at doi:10.1016/j.clinph.2009.08.018.

References

Amunts K, Zilles K. Advances in cytoarchitectonic mapping of the human cerebral cortex. Neuroimaging Clin N Am 2001;11(2):151–69.
Barth DS, Sutherling W, Broffman J, Beatty J. Magnetic localisation of a dipolar current source implanted in a sphere and a human cranium. Electroencephalogr Clin Neurophysiol 1986;63:260–73.
Bragin A, Engel Jr J, Wilson CL, Fried I, Mathern GW. Hippocampal and entorhinal cortex high-frequency oscillations (100–500 Hz) in human epileptic brain and in kainic acid-treated rats with chronic seizures. Epilepsia 1999;40(2):127–37.
Bragin A, Wilson CL, Staba RJ, Reddick M, Fried I, J Jr Engel. Interictal high-frequency oscillations (80–500 Hz) in the human epileptic brain: entorhinal cortex. Ann Neurol 2002;52(4):407–15.
Brookes MJ, Stevenson CM, Barnes GR, Hillebrand A, Simpson MI, Francis ST, Morris PG. Beamformer reconstruction of correlated sources using a modified source model. Neuroimage 2007;34:1454–65.
Cracco RQ, Cracco JB. Somatosensory evoked potential in man: far field potentials. Electroencephalogr Clin Neurophysiol 1976;41(5):460–6.
Curio G, Mackert BM, Burghoff M, Koetitz R, Abraham-Fuchs K, Härer W. Localisation of evoked neuromagnetic 600 Hz activity in the cerebral somatosensory system. Electroencephalogr Clin Neurophysiol 1994;91(6):483–7.
Curio G, Mackert BM, Burghoff M, Neumann J, Nolte G, Scherg M, et al. Somatotopic source arrangement of 600 Hz oscillatory magnetic fields at the human primary somatosensory hand cortex. Neurosci Lett 1997;234(2–3):131–4.
Darvas F, Pantazis D, Kucukaltun-Yildirim E, Leahy RM. Mapping human brain function with MEG and EEG: methods and validation. Neuroimage 2004;23:S289–99.
Eickhoff S, Stephan KE, Mohlberg H, Grefkes C, Fink GR, Amunts K, et al. A new SPM toolbox for combining probabilistic cytoarchitectonic maps and functional imaging data. Neuroimage 2005;25(4):1325–35.
Eickhoff SB, Heim S, Zilles K, Amunts K. Testing anatomically specified hypotheses in functional imaging using cytoarchitectonic maps. Neuroimage 2006;32(2):570–82.
Eickhoff SB, Paus T, Caspers S, Grosbras MH, Evans A, Zilles K, et al. Assignment of functional activations to probabilistic cytoarchitectonic areas revisited. Neuroimage 2007;36(3):511–21.
Eisen A, Roberts K, Low M, Hoirch M, Lawrence P. Questions regarding the sequential neural generator theory of the somatosensory evoked potential raised by digital filtering. Electroencephalogr Clin Neurophysiol 1984;59(5):388–95.

Fieseler T, Ioannides AA, Liu MJ, Nowak, H. A numerically stable approximation for the magnetic field of the conducting spheroid close to the symmetry axis. In: Aine C, Okada Y, Stroink G, Swithenby S, Wood C, editors. BIOMAG – Proceedings of the 10th international conference on biomagnetism, vol. 1, Springer; 1996. p. 209–212.

Gobbelé R, Buchner H, Curio G. High-frequency (600 Hz) SEP activities originating in the subcortical and cortical human somatosensory system. Electroencephalogr Clin Neurophysiol 1998;108(2):182–9.

Gobbelé R, Buchner H, Scherg M, Curio G. Stability of high-frequency (600 Hz) components in human somatosensory evoked potentials under variation of stimulus rate-evidence for a thalamic origin. Clin Neurophysiol 1999;110(9):1659–63.

Gobbelé R, Waberski TD, Simon H, Peters E, Klostermann F, Curio G, et al. Different origins of low- and high-frequency components (600 Hz) of human somatosensory evoked potentials. Clin Neurophysiol 2004;115(4):927–37.

Gross J, Ioannides AA. Linear transformations of data space in MEG. Phys Med Biol 1999;44:2081–97.

Hamalainen M, Hari R, Ilmoniemi RJ, Knuutila J, Lounasmaa OV. Magnetoencephalography – theory, instrumentation, and applications to noninvasive studies of the working human brain. Rev Mod Phys 1993;65(2):413–97.

Hansen JS, Ko HW, Fisher RS, Litt B. Practical limits on the biomagnetic inverse process determined from in vitro measurements in spherical conducting volumes. Phys Med Biol 1988;33:105–11.

Hashimoto I. Exploring the neural mechanisms of high-frequency oscillation (300–900 Hz) from the human somatosensory cortex. NeuroReport 2001;12(2):A7.

Hashimoto I, Kimura T, Fukushima T, Iguchi Y, Saito Y, Terasaki O, Sakuma K. Reciprocal modulation of somatosensory evoked N20m primary response and high-frequency oscillations by interference stimulation. Clin Neurophysiol 1999;110(8):1445–51.

Hashimoto I, Mashiko T, Imada T. Somatic evoked high-frequency magnetic oscillations reflect activity of inhibitory interneurons in the human somatosensory cortex. Electroencephalogr Clin Neurophysiol 1996;100(3):189–203.

Haueisen J, Heuer T, Nowak H, Liepert J, Weiller C, Okada Y, et al. The influence of lorazepam on somatosensory-evoked fast frequency (600 Hz) activity in MEG. Brain Res 2000;874(1):10–4.

Haueisen J, Schack B, Meier T, Curio G, Okada Y. Multiplicity in the high-frequency signals during the short-latency somatosensory evoked cortical activity in humans. Clin Neurophysiol 2001;112(7):1316–25.

Hironaga N, Ioannides AA. Accurate co-registration for MEG reconstructions. In: Nowak H, Haueisen J, Giessler F, Huonker R, editors. Proceedings of the 13th International Conference on Biomagnetism, Berlin, VDE Verlag; 2002. p. 931–933.

Huang MX, Mosher JC, Leahy RM. A sensor-weighted overlapping-sphere head model and exhaustive head model comparison for MEG. Phys Med Biol 1999;44:423–40.

Huiskamp G, Vroeijenstijn M, van Dijk R, Wieneke G, van Huffelen AC. The need for correct realistic geometry in the inverse EEG problem. IEEE Trans Biomed Eng 1999;46:1281–7.

Ioannides AA, Bolton JPR, Clarke CJS. Continuous probabilistic solutions to the biomagnetic inverse problem. Inverse problem 1990;6:523–42.

Ioannides AA, Kostopoulos GK, Laskaris NA, Liu L, Shibata T, Schellens M, et al. Timing and connectivity in the human somatosensory cortex from single trial mass electrical activity. Hum Brain Mapp 2002;15:231–46.

Jirsch JD, Urrestarazu E, LeVan P, Olivier A, Dubeau F, Gotman J. High-frequency oscillations during human focal seizures. Brain 2006;129(Pt 6):1593–608.

Jones MS, Barth DS. Spatiotemporal organization of fast (>200 Hz) electrical oscillations in rat Vibrissa/Barrel cortex. J Neurophysiol 1999;82(3):1599–609.

Jones MS, Barth DS. Effects of bicuculline methiodide on fast (>200 Hz) electrical oscillations in rat somatosensory cortex. J Neurophysiol 2002;88(2):1016–25.

Jones MS, MacDonald KD, Choi B, Dudek FE, Barth DS. Intracellular correlates of fast (>200 Hz) electrical oscillations in rat somatosensory cortex. J Neurophysiol 2000;84(3):1505–18.

Laskaris NA, Ioannides AA. Exploratory data analysis of evoked response single trials based on minimal spanning tree. Clin Neurophysiol 2001;112(4):698–712.

Laskaris NA, Liu LC, Ioannides AA. Single-trial variability in early visual neuromagnetic responses: an explorative study based on the regional activation contributing to the N70m peak. Neuroimage 2003;20:765–83.

Leahy RM, Mosher JC, Spencer ME, Huang MX, Lewine JD. A study of dipole localisation accuracy for MEG and EEG using a human skull phantom. Electroencephalogr Clin Neurophysiol 1998;107:159–73.

Lee TW, Girolami M, Sejnowski TJ. Independent component analysis using an extended INFOMAX algorithm for mixed sub-Gaussian and super-Gaussian sources. Neural Comput 1999;11:606–33.

Liljestrom M, Kujala J, Jensen O, Salmelin R. Neuromagnetic localisation of rhythmic activity in the human brain: a comparison of three methods. Neuroimage 2005;25:734–45.

Liu L, Ioannides AA. A correlation study of averaged and single trial MEG signals: the average describes multiple histories each in a different set of single trials. Brain Topogr 1996;8:385–96.

Liu LC, Ioannides AA, Mueller-Gaertner HW. Bi-hemispheric study of single trial MEG signals of the human auditory cortex. Electroencephalogr Clin Neurophysiol 1998;106:64–78.

Makeig S, Westerfield M, Jung TP, Enghoff S, Townsend J, Courchesne E, et al. Dynamic brain sources of visual evoked responses. Science 2002;295:690–4.

Mosher JC, Lewis PS, Leahy RM. Multiple dipole modeling and localisation from spatio-temporal MEG data. IEEE Trans Biomed Eng 1992;39:541–57.

Norra C, Waberski TD, Kawohl W, Kunert HJ, Hock D, Gobbelé R, et al. High-frequency somatosensory thalamocortical oscillations and psychopathology in schizophrenia. Neuropsychobiology 2004;49(2):71–80.

Ozaki I, Suzuki C, Yaegashi Y, Baba M, Matsunaga M, Hashimoto I. High frequency oscillations in early cortical somatosensory evoked potentials. Electroencephalogr Clin Neurophysiol 1998;108(6):536–42.

Papadelis C, Ioannides AA. Localisation accuracy and temporal resolution of MEG: a phantom experiment. Int Cong Ser 2007;1300:257–60.

Phillips JW, Leahy RM, Mosher JC. MEG-based imaging of focal neuronal current sources. IEEE Trans Med Imaging 1997;16:338–48.

Poghosyan V, Ioannides AA. Precise mapping of early visual responses in space and time. Neuroimage 2007;35:759–70.

Robinson S, Vrba J. Functional neuroimaging by synthetic aperture magnetometry. In: Yoshimoto T, Kotani M, Kuriki S, Karibe H, Nakasato N, editors. Recent advances in biomagnetism, Sendai, Tohoku Univ. Press; 1998. p. 302–305.

Salenius S, Portin K, Kajola M, Salmelin R, Hari R. Cortical control of human motoneuron firing during isometric contraction. J Neurophysiol 1997;77:3401–5.

Salmelin R, Hari R. Characterization of spontaneous MEG rhythms in healthy adults. Electroencephalogr Clin Neurophysiol 1994;91:237–48.

Salmelin R, Sams M. Motor cortex involvement during verbal versus non-verbal lip and tongue movements. Hum Brain Mapp 2002;16:81–91.

Salmelin R, Schnitzler A, Schmitz F, Freund HJ. Single word reading in developmental stutterers and fluent speakers. Brain 2000;123:1184–202.

Sarvas J. Basic mathematical and electromagnetic concepts of the biomagnetic inverse problem. Phys Med Biol 1987;32:11–22.

Staba RJ, Wilson CL, Bragin A, Fried I, Engel Jr J. Quantitative analysis of high-frequency oscillations (80–500 Hz) recorded in human epileptic hippocampus and entorhinal cortex. J Neurophysiol 2002;88(4):1743–52.

Sutherling WW, Akhtari M, Mamelak AN, Mosher J, Arthur D, Sands S, et al. Dipole localisation of human induced focal afterdischarge seizure in simultaneous magnetoencephalography and electrocorticography. Brain Topogr 2001;14:101–16.

Taniguchi M, Kato A, Fujita N, Hirata M, Tanaka H, Kihara T, et al. Movement-related desynchronization of the cerebral cortex studied with spatially filtered magnetoencephalography. Neuroimage 2000;12:298–306.

Taylor JG, Ioannides AA, Muller-Gartner HW. Mathematical analysis of lead field expansions. IEEE Trans Med Imaging 1999;18:151–63.

Uitert RV, Johnson C. Can a spherical model substitute for a realistic head model in forward and inverse MEG simulations? In: Proc Conf Biomagnetism, Jena, Germany; 2002.

Vrba J, Cheung T, Cheyne D, Robinson SE, Starr A. Errors in ECD localization with partial sensor coverage. In: Yoshimoto T, Kotani M, Kuriki S, Karibe H, Nakasato N, editors. Recent advances in biomagnetism. Sendai, Japan, Tohoku Univ. Press; 1999. p. 109–112.

Vrba J, Robinson SE. Linear constrained minimum variance beamformers, synthetic aperture magnetometry, and MUSIC in MEG applications. In: Conference Record of the 34th Asilomar Conference on Signal, System, and Computers, vol. 1; 2000. p. 331–337.

Vrba J, Robinson SE. Signal processing in magnetoencephalography. Methods 2001;25:249–71.

von Helmholtz H. Uber einige gesetze der verthheilung elektrischer strome in korperlichen leitern, mit anwendung auf die thierischelektrischen versuche. Ann Phys Chem 1853;89:353–77.

Yamada T, Kameyama S, Fuchigami Y, Nakazumi Y, Dickins QS, Kimura J. Changes of short latency somatosensory evoked potential in sleep. Electroencephalogr Clin Neurophysiol 1988;70(2):126–36.

Yamamoto T, Williamson SJ, Kaufman L, Nicholson C, Llinas R. Magnetic localisation of neuronal activity in the human brain. Proc Natl Acad Sci 1988;85:8732–6.